Journal of Alloys and Compounds 520 (2012) 244–249

Contents lists available at SciVerse ScienceDirect

Journal of Alloys and Compounds

journal homepage: www.elsevier.com/locate/jallcom

Effects of Ti addition to Sn–Ag and Sn–Cu solders

W.M. Chen [a], S.K. Kang [b], C.R. Kao [a,*]

[a] Department of Materials Science and Engineering, National Taiwan University, Taipei, Taiwan
[b] IBM T. J. Watson Research Center, Yorktown Heights, New York, USA

ARTICLE INFO

Article history:
Received 9 November 2011
Received in revised form 3 January 2012
Accepted 4 January 2012
Available online 13 January 2012

Keywords:
Minor alloying elements
Pb-free solders
Ti addition

ABSTRACT

Minor alloying addition to solders has been an important strategy to improve the integrity and reliability of Pb-free solder joints. In this study, a small amount of Ti was added to Sn–Cu and Sn–Ag solders, and their microstructures, solidification behaviors, mechanical properties, and high temperature aging characteristics were investigated. Thermal analysis confirmed Ti addition being very effective in reducing the undercooling. Correlations between cooling rates, microstructure, and microhardness were established. One pronounced feature of Ti addition was that Ti-added solders had microstructures very stable against extreme aging conditions.

© 2012 Elsevier B.V. All rights reserved.

1. Introduction

Near-eutectic Sn–Ag–Cu (SAC) solders are the most popular solders for surface mount technology (SMT) or ball grid array (BGA) applications [1,2]. However, SAC solders, because of their high moduli, are not very adequate for certain applications requiring high impact strength, such as in mobile electronics. In addition, their high joint strength often yields a serious chip joining problem such as chip-to-package interaction (CPI) or white bump defects in a back-end-of-line (BEOL) structure. Consequently, using SAC solders with a low Ag or Cu content becomes a trend in mobile electronics or flip-chip interconnects. However, lowering the modulus or strength by reducing Ag or Cu content in SAC solders creates another reliability concern: a reduction in electromigration resistance in high-performance flip chip joints where a high current carrying property is required. Therefore, a search for new Pb-free solders with balanced properties is an urgent issue. In a series of studies, binary Sn–Ag and Sn–Cu solders were systematically investigated for flip-chip packaging applications [3–6].

Only recently have a considerable number of studies been conducted on the beneficial effects of minor alloying elements in Sn-rich solders. The investigated minor alloying elements include Co, Cu, Fe, Ni, Zn and others [1,7–16]. Many of the effective minor alloying elements are transition metals whose atoms have an incomplete d sub-shell and therefore can easily form many kinds of intermetallic compounds (IMCs) with other metals. These active elements are believed to be the most beneficial additives regarding modifying Pb-free solders to improve significantly their joint properties.

Liu et al. [17] were the first to add Ti, one of the most active transition metals, into SAC as a minor element. Titanium addition yielded a superior drop-test performance by reducing elastic modulus. This improvement in drop test performance did not compromise the thermal creep performance which usually turns into a concern as the drop test performance is improved. Furthermore, a dramatic suppression of the undercooling of SAC and a reduced growth of interfacial IMCs were reported in that study. They presumed that Ti could be considered as the most promising candidate among other alloying elements. However, Vuorinen et al. [18] recently reported a long-term aging experiment on the interfacial reaction between the eutectic SnAg with 1 at.% Ti added and Cu. They found the interfacial IMC growth was not affected by Ti-addition. They also argued that since Ti has an extremely low solubility to Sn–Ag solder and to Cu–Sn IMCs, the minor addition of Ti cannot change activities of components in the solder nor influence the stability of the IMC layers. Since the above-mentioned two papers do not report consistent observations, a systematic inquiry is needed to clarify the effect of Ti-addition to Sn-rich solders. In this study, we carry out a series of experiments on Sn–Ag and Sn–Cu solders with Ti-addition to uncover their solidification behavior, microstructure, interfacial reactions, mechanical properties, resistance to electro-migration and others. This paper is the first part of our

* Corresponding author.
E-mail address: crkao@ntu.edu.tw (C.R. Kao).

0925-8388/$ – see front matter © 2012 Elsevier B.V. All rights reserved.
doi:10.1016/j.jallcom.2012.01.032

Table 1
Collection of peak temperatures (°C) and undercooling (ΔT) in DSC analysis for Sn–Ag and Sn–Cu base solders.

	Heating process		Cooling process		Undercooling
	T_p (eutectic)	T_p (β-Sn)	T_p (eutectic)	T_p (β-Sn)	ΔT (β-Sn)
Sn–0.5Ag	224.5	230.3	213.6		16.7
Sn–1.0Ag	224.5	230.2	190.7		39.5
Sn–1.0Ag–0.2Ti	224.5	230.8	218.9	227.7	3.1
Sn–1.0Ag–0.6Ti	224.4	230.6	219.3	227.9	2.7
Sn–0.7Cu	229.4		194.9		34.5
Sn–0.7Cu–0.2Ti	230.2		226.3		3.9
Sn–0.7Cu–0.6Ti	230.2		226.6		3.6

on-going research, reporting mainly the solidification, undercooling, microstructure, mechanical properties and high temperature aging characteristics of Sn–Ag and Sn–Cu solders alloyed with Ti.

2. Experimental procedures

Two binary Sn-rich solders are chosen as the master alloys: Sn–1.0Ag (wt.%) (SA) and Sn–0.7Cu (wt.%) (SC). Different amounts of Ti were added into SA and SC, producing four different Ti-bearing alloys with the following compositions: Sn–1.0Ag–0.2Ti (SA0.2Ti), Sn–1.0Ag–0.6Ti (SA0.6Ti), Sn–0.7Cu–0.2Ti (SC0.2Ti), and Sn–0.7Cu–0.6Ti (SC0.6Ti). Some solder samples were also produced in the form of small solder cylinders by the method of injection molded solder (IMS) [19]. The solder cylinders have a diameter of 294 μm (12 mil) and a length of 381 μm (15 mil).

Differential scanning calorimeter (DSC) was employed to reveal intrinsic thermal behavior. During DSC measurements, solders of approximate 5 mg weight were heated up and cooled down at a constant rate of 6 °C/min under a nitrogen atmosphere. By observing the endothermic and exothermic heat flows, the melting and solidification behaviors as well as the undercooling were analyzed. Undercooling is one of the important features that affect the reliability of solder joints by causing non-uniform solidification among many neighboring solder joints.

To investigate the effect of cooling rates on microstructure, three cooling rates were used: furnace-cooling, air cooling and water-quenching. The solders were molten at 250 °C for 10 min under a nitrogen atmosphere and then subjected to furnace-cooling, air-cooling or water-quenching afterward. Optical microscopy (OM) was employed to produce both bright field and cross-polarized images for microstructure information.

Vickers hardness (VH) data were obtained by using 5 g force and 5 s dwell time on well-polished surface of solders. Each VH value in this paper was reported as an average of at least 20 indentations.

3. Results and discussion

3.1. Melting, solidification and undercooling of Ti-alloyed solders

Vertices in DSC data signify local-strongest heat flows and indicate phase transitions occurring during the heating and cooling cycles as shown in Fig. 1. The valleys in a heating curve of DSC stand for intense endothermic phase transitions (melting) whereas the peaks in a cooling procedure represent strong exothermal phase transitions (solidification). Due to the overlap between eutectic and β-Sn vertices in DSC, the onset temperature is difficult to be obtained precisely, therefore the peak temperatures were employed in this study. The values in Table 1 are the peak temperatures for each vertex, showing a collection of DSC data. Inspecting the undercooling of four solders, it is found that minor Ti addition effectively reduces the amount of the undercooling of Sn-rich solders, and more Ti addition can only slightly reduce the undercooling further. This result is quite consistent with the explanation proposed by Cho et al. [20] that alloying elements with a hexagonal closed packed (hcp) structure may enhance the heterogeneous nucleation of β-Sn and thereby reducing its undercooling.

Fig. 1(a) and (b) shows the melting and freezing DSC data of Ag-containing solders, respectively. One may notice that, during heating, Fig. 1(a) shows that there are two valleys in each Ag-containing solder. The two valleys are found to be associated with the melting heat flows coming from eutectic Sn–Ag and β-Sn,

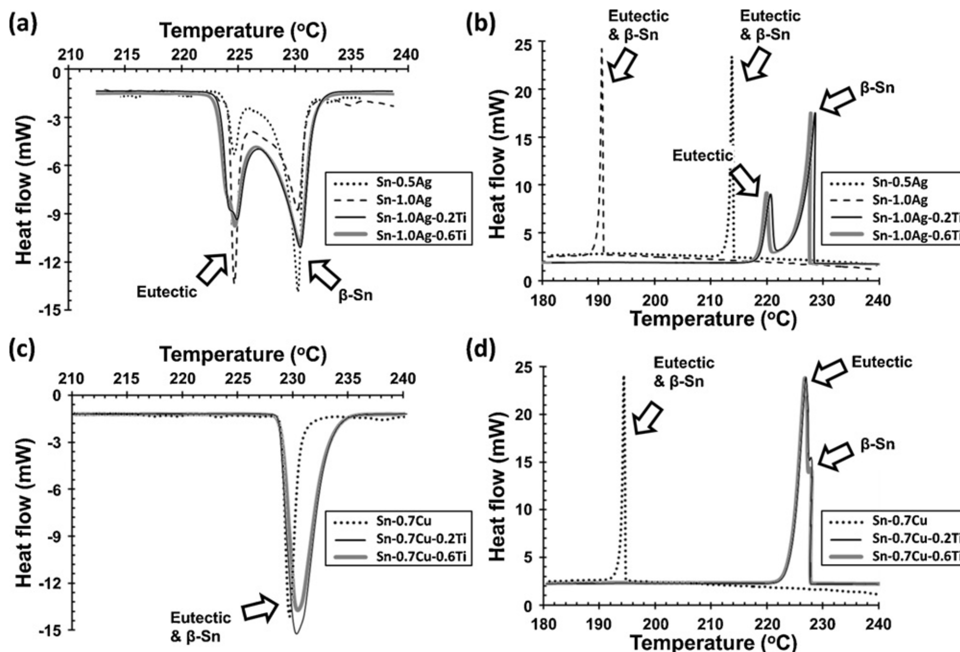

Fig. 1. Differential scanning calorimetery (DSC) results of Sn–Ag and Sn–Ag–Ti solders (a) during heating (endothermal) and (b) during cooling (exothermal). DSC results of Sn–Cu and Sn–Cu–Ti solders (c) during heating (endothermal) and (d) during cooling (exothermal).

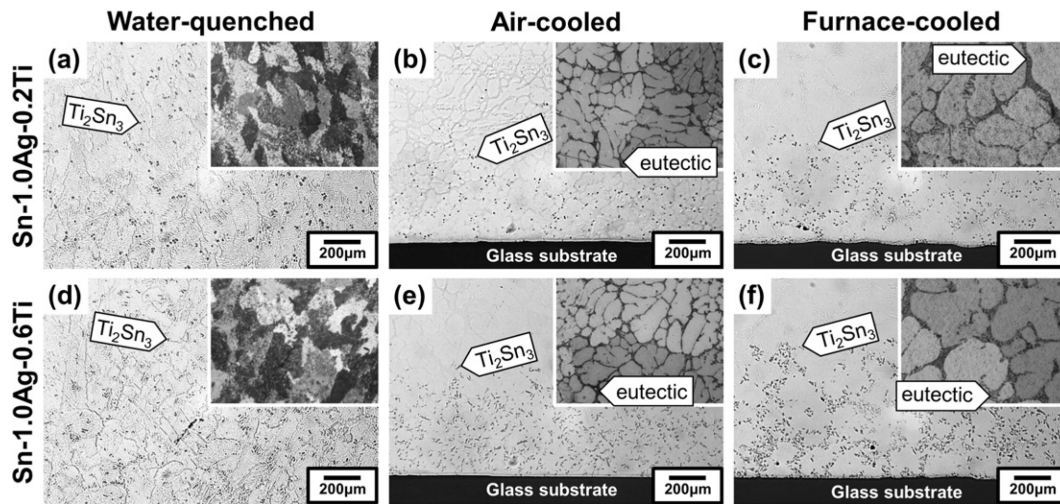

Fig. 2. Optical microscopy (OM) bright filed and cross-polarized images of Sn–Ag–Ti solders as a function of cooling rate and Ti concentration.

respectively. Considering the eutectic composition of Sn–3.5Ag (wt.%), Sn–0.5Ag and Sn–1.0Ag (SA) used in this study are hypoeutectic. Minor Ti addition is expected not to change the composition too much, so SA0.2Ti and SA0.6Ti can be seen as hypoeutectic comprising SnAgTi eutectic and β-Sn phase. When the solder is heated up to its eutectic temperature (T_e), the eutectic phase melts first and generates the first endothermic vertex. As long as the temperature keeps increasing, the β-Sn phase starts melting and causes the second vertex, and the two-vertices appearance therefore manifested during DSC heating process.

However, in the case of cooling, only Ti-added solders have the two-vertices appearance as shown in Fig. 1(b). This is owing to the small undercooling of Ti-added solders permitting two close vertices shown separately in a continuous DSC examination. For the solders without Ti, their undercooling is so large that the actual solidification temperature of β-Sn is even lower than the equilibrium freezing temperature of eutectic phase and this freezing of β-Sn is believed to occur almost simultaneously as the solidification of the eutectic phase. As shown in Fig. 1(b), only one peak can be observed in pure Sn–0.5Ag and Sn–1.0Ag because their undercooling was magnificent. It is worth noting that undercooling is also the reason why the peak temperatures in Fig. 1(b) are much lower than in Fig. 1(a).

In the case of Cu-containing solder, the liquidus temperature of β-Sn is very close to T_e due to its near-eutectic composition. As shown in Fig. 1(c), during heating, in no way can one tell the difference of liquidus temperature between the eutectic and β-Sn. Nevertheless, during cooling, Fig. 1(d) shows that one can distinguish a small peak beside the main peak either in SC0.2Ti or in SC0.6Ti whereas only one peak was observed in the SC without Ti. The reason is similar to what was discussed for the Ag-containing case; Ti addition reduces the undercooling much enough that each peak can be defined clearly during the freezing sequence. All these observations imply that a small amount of Ti addition to Sn-rich solders will significantly change their microstructure by the large reduction in the undercooling during solidification of solder joints. Namely, the solders without Ti are usually finer in microstructure than the Ti-added ones because of the large undercooling.

3.2. Effect of cooling rate on microstructure and mechanical properties

Water-quenching (>100 °C/s), air-cooling (∼10 °C/s) and furnace-cooling (∼0.01 °C/s) were applied during solidification of SA0.2Ti, SA0.6Ti, SC0.2Ti and SC0.6Ti solders after reflow at 250 °C, 10 min. Figs. 2 and 3 are the cross-section images of solders as a

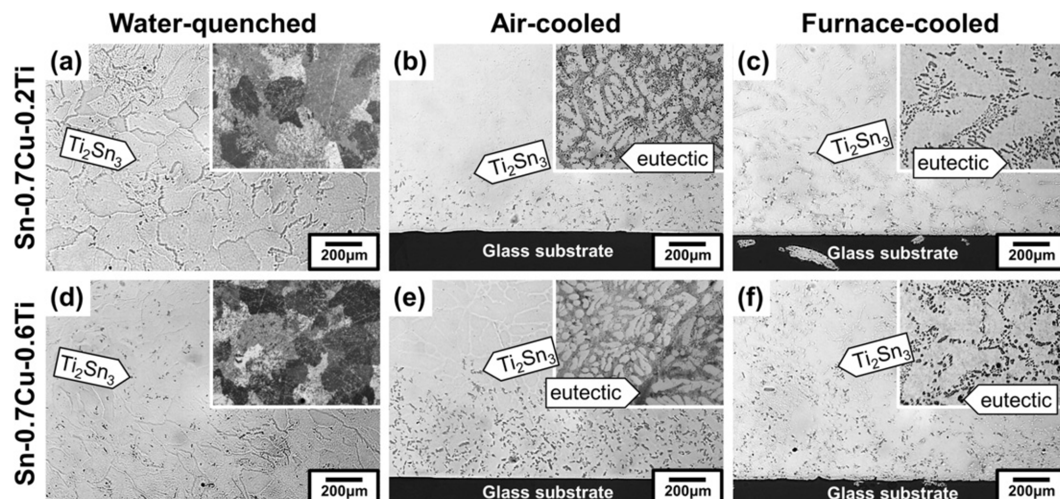

Fig. 3. OM bright filed and cross-polarized images of Sn–Cu–Ti solders as a function of cooling rate and Ti concentration.

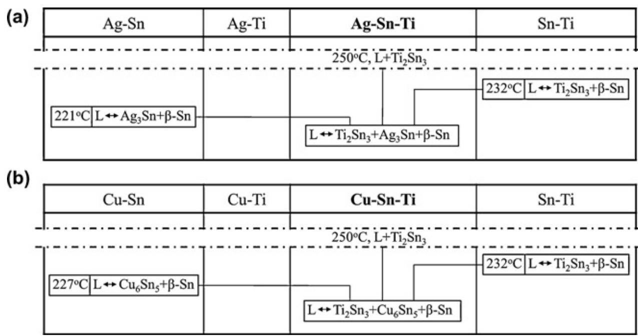

Fig. 4. Reaction schemes drawn for minor Ti alloyed (a) Sn–Ag solders and (b) Sn–Cu solders.

function of cooling rate and Ti concentration. OM bright filed and cross-polarized images are employed to analyze the microstructure of β-Sn grains and β-Sn dendrites. OM bright field images can reveal both grain boundaries and dendrite cell boundaries, but cannot distinguish them. However, cross-polarized images can tell different grain orientations and define grain boundaries, as shown in the upper-right inserts of each condition in Figs. 2 and 3.

Fig. 2 shows the microstructure of SA0.2Ti and SA0.6Ti solders. According to energy-dispersive X-ray spectroscope (EDS), the darker contrast precipitates and the dense phase in between β-Sn were identified as Ti_2Sn_3 and SnAgTi eutectic, respectively. Fig. 2(a) shows that, besides shrinking β-Sn grain size, water-quenching had Ti_2Sn_3 intermetallics dispersed randomly inside the solder. The solder was water-quenched so rapidly that Ti_2Sn_3 particles were frozen and kept dispersive similarly as in molten solder. In the case of slower cooling, such as air- and furnace-cooling, as shown in Fig. 2(b) and (c), Ti_2Sn_3 were found near the bottom side of the solder which was directly in contact with a glass substrate. Because of high heat conduction, the solidification would start at the glass substrate. Fig. 4 shows the reaction schemes drawn for Ti alloyed Sn–Ag and Sn–Cu [21,22] solders based on the liquidus surface for primary solidification. According to Fig. 4(a), even though the Sn–Ag–Ti solder matrix is molten under 250 °C reflow, Ti_2Sn_3 segregates as solid precipitates. That is, Ti_2Sn_3 will form prior to the solidification of Sn–Ag–Ti and tend to congregate at the lower temperature area during solidification. In this case, Ti_2Sn_3 moved to the bottom part owing to the lower temperature and being jostled to β-Sn grain boundaries or dendrite cell boundaries. It is worth noting that the density of Ti_2Sn_3 is 7.184 g/cm^3 according to Kleinke et al. [23] and the density of molten Sn solder near melting point is about 6.99 g/cm^3 [24]. Thus, the density variation is quite small and its effect on the distribution of Ti_2Sn_3 in molten Sn would be insignificant due to the effect of turbulent flow in molten solder.

When the Ti concentration in solders increases to 0.6 wt.% as shown in Fig. 2(d)–(f), the number of Ti_2Sn_3 precipitates increases accordingly and they become coarser and denser. By SEM-EDS analysis, it is found that when Ti_2Sn_3 particles become coarse enough, their central composition changes into Ti_6Sn_5. The alteration of Ti concentration in solder is expected to change the chemical potential of solders and may shift the interfacial reactions during soldering. Further experimental study is on-going to verify this assumption.

Shown in Fig. 3 is the bright field and cross-polarized images of SC0.2Ti and SC0.6Ti. The major influence of cooling rates on Sn–Cu–Ti and Sn–Ag–Ti are very similar, i.e., with a higher cooling rate, β-Sn will become finer as well as diverse in orientations. From a thermodynamic perspective, only minor Ti was added into SC which is eutectic composition, so SC0.2Ti and SC0.6Ti can be reasonably regarded as the near-eutectic composition. Compared Sn–Cu–Ti with Sn–Ag–Ti, quantitative analyses from cross-section images (Figs. 2 and 3) also suggest the ratio of eutectic to β-Sn in Sn–Cu–Ti is higher than in Sn–Ag–Ti. This result consists with the fact that Sn–Cu–Ti is the near-eutectic while Sn–Ag–Ti is hypoeutectic. Consequently, a higher strength or hardness is expected in Sn–Cu–Ti due to more eutectic phases existing. This is confirmed by the microhardness test to be discussed later.

The cross-polarized inserts in Figs. 2 and 3 show that β-Sn grains in Sn–Cu–Ti are generally larger than in Sn–Ag–Ti regardless of dendrite population. Moreover, β-Sn grain orientations in Sn–Cu–Ti are less divergent than in Sn–Ag–Ti. These results are consistent with the previous study [4] which focused on pure SC and SA, and implying that the tendency of orientation distribution of β-Sn in SC and SA can be preserved after a minor addition of Ti.

Fig. 5 shows the microhardness results of Sn–Ag and Sn–Cu base solders as a function of cooling condition. In general, compared with Figs. 2 and 3, a faster cooling rate would produce a finer microstructure and also a higher hardness. This concept has been well interpreted by Hall–Petch equation associated with the dislocation theory assuming that grain boundaries act as obstacles to slip dislocations. Nevertheless, pure Sn–1.0Ag seems not to obey this rule and manifests the maximum hardness when it was air-cooled. This can be attributed to a higher amount of Ag_3Sn precipitates in air-cooled Sn–1.0Ag. Although the microstructure of β-Sn in air-cooled Sn–1.0Ag is coarser than in water-quenched one, Ag_3Sn which is the main contributor to hardness can fully segregate along Sn dendrite cell boundaries as well as Sn grain boundaries, forming abundant networks in air-cooled samples. These Ag_3Sn networks are believed to strengthen solders more efficiently than the grain refinement made by a faster cooling rate. In the case of water-quenched Sn–1.0Ag, the solidification is so fast that most Ag atoms are supersaturated into Sn solid solution, not to diffuse out of the solder matrix or to precipitate as Ag_3Sn. Hence, the formation of Ag_3Sn networks would be greatly suppressed in this case.

Ti-added Sn–1.0Ag solders (SnAg0.2Ti and SnAg0.6Ti), however, abide by the prediction of grain refinement strengthening. This is because, either in SnAg0.2Ti or SnAg0.6Ti, the Ti_2Sn_3 IMCs are mainly responsible for hardening, not by Ag_3Sn. And according to

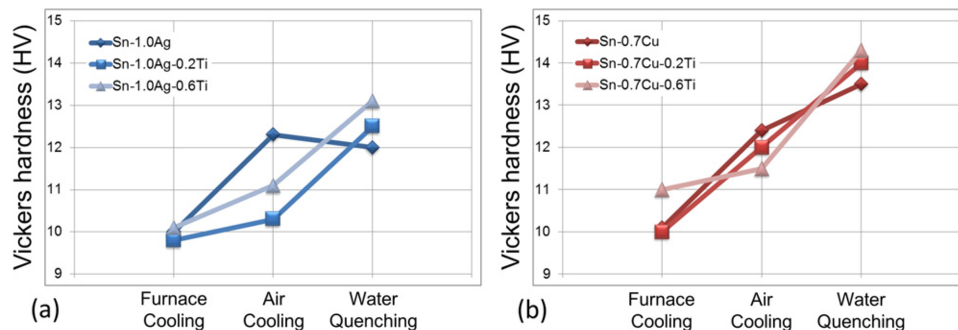

Fig. 5. Illustration of microhardness results of (a) Sn–Ag and (b) Sn–Cu base solders undergoing different cooling conditions.

Fig. 6. OM bright filed images of SA0.2Ti, SA0.6Ti, SC0.2Ti and SC.6Ti solders aged at 200 °C for 0 h, 2 h, 30 h and 100 h.

Fig. 4(a) and (b), Ti_2Sn_3 has already formed and well distributed in the molten solder matrix either in Sn–Ag or in Sn–Cu before solidification, so the amount of Ti_2Sn_3 is decided only by Ti concentration in solders instead of by cooling rate. That is, in Sn–Ag–Ti solder system, the size of β-Sn grain and dendrite becomes a decisive factor in controlling intrinsic hardness of solders. This suggests that the faster cooling rate, the finer microstructure, and the higher hardness accordingly.

3.3. High temperature aging characteristics

Since the melting temperature of SA and SC are about 220–230 °C, the aging chosen at 200 °C is an extreme condition which can massively accelerate diffusion process in solid state. The self-diffusivity of Sn in 200 °C is about 23-times as much as in 150 °C according to Arrhenius equation for mass-diffusion [25]. Shown in Fig. 6 is a matrix of magnified images of Ti_2Sn_3 networks precipitating in solders. The first column shows the initial state before aging for each composition. The cross-section images indicate that, after air-cooling, Ti_2Sn_3 particles will locate as colonies at dendrite cell boundaries or grain boundaries area either in SC or SA. When 200 °C aging was applied, unexpectedly, on no account did Ti_2Sn_3 grow or coarsen. Ti_2Sn_3 particles and networks are quite stable and almost unchanged even after 100 h aging. While Ti_2Sn_3 has been stabilized during aging, the eutectic phase dispersed in solders, however, coarsened and aggregated together easily. This can be confirmed by

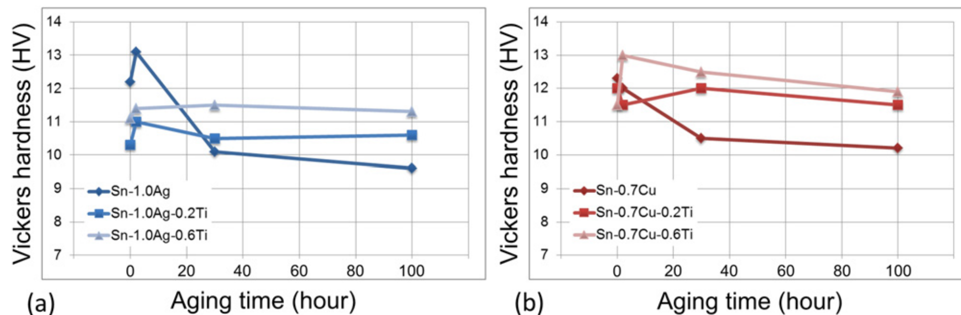

Fig. 7. Illustration of microhardness results of (a) Sn–Ag and (b) Sn–Cu base solders aged at 200 °C up to 100 h.

Fig. 6(m)–(p), showing the sequence of the event in SC0.6Ti during the aging for the time up to 100 h. In Fig. 6(p), the darker particles are Ti_2Sn_3 whereas the brighter ones are identified as SnCuTi IMCs which are believed to be congregated from the eutectic phase.

Although the eutectic phase becomes coarsened during aging, stable Ti_2Sn_3 networks can effectively firm the morphology of β-Sn by retarding its growth. In our previous study [4], when pure SA and SC were aged at 200 °C for 8 h, both β-Sn dendrites and β-Sn grains grew remarkably. In this study, the average size of β-Sn in Ti-added solders did not change even after 100 h aging. Accordingly, it could be claimed that the Sn diffusion is suppressed by the minor Ti addition. And this also implies Ti-added solder may be a good candidate for enhanced electro-migration resistance, which is a vital issue in high performance solder interconnections. Experiments on EM testing with Ti-alloyed solders are also on-going.

Fig. 7 shows the microhardness data of Sn–Ag base and Sn–Cu base solders as a function of aging time. The results unequivocally proved that the Ti addition can stabilize either Sn–Ag or Sn–Cu base solders even under a severe aging condition. In Fig. 7(a), it is worth noting that, at the initial stage of aging, the early increase in hardness for Sn–Ag solders (not for Sn–Cu) may be due to precipitation of supersaturated Ag atoms into Ag3Sn particles forming a strong network of IMCs. As the aging time increases, a steep drop of hardness is noticed in Sn–1.0Ag, not in the Ti-added Sn–Ag. For the Sn–Cu solders, the hardness values are again very stable for Ti-added solders, but not for Sn–Cu without Ti addition.

4. Conclusions

Ti additions to Sn–Cu and Sn–Ag solders can effectively reduce the undercooling of solders, and thereby alter their microstructure by changing the solidification behavior. Microhardness analysis of Sn–Cu–Ti and Sn–Ag–Ti solders confirms that the faster cooling speed, the finer microstructure, and the higher the hardness. However, this trend does not apply to Sn–1.0Ag where Ag3Sn precipitate network controls its major hardening. For Ti-added solders, when exposed to a severe aging condition, although eutectic phases become coarsened, Ti_2Sn_3 networks can stabilize the morphology of β-Sn by retarding their grain growth, and maintain the strength of solders.

Acknowledgement

The authors would like to thank M.H. Lu, P.A. Lauro, J.W. Nah and K.W. Lee for useful discussion and sample preparation. We are also grateful to T.C. Chen and F. Claudius for arranging this collaboration. This work was supported by National Science Council of Taiwan through grant NSC 99-2911-I-002-100 and International Business Machines Corporation.

References

[1] S.K. Kang, A.K. Sarkhel, J. Electron. Mater. 23 (1994) 701.
[2] S.K. Kang, W.K. Choi, D.Y. Shih, D.W. Henderson, T. Gosselin, A. Sarkhel, C. Goldsmith, K.J. Puttlitz, IEEE Electron. Compon. Technol. Conf. 53 (2003) 64.
[3] M. Lu, D.Y. Shih, P. Lauro, C. Goldsmith, D.W. Henderson, Appl. Phys. Lett. 92 (2008) 211909.
[4] S.K. Seo, S.K. Kang, D.Y. Shih, H.M. Lee, Microelectron. Reliab. 49 (2009) 288.
[5] S.K. Seo, S.K. Kang, D.Y. Shih, H.M. Lee, J. Electron. Mater. 38 (2009) 257.
[6] S.K. Seo, S.K. Kang, M.G. Cho, H.M. Lee, JOM 62 (2010) 22.
[7] I.E. Anderson, J.C. Foley, B.A. Cook, J. Harringa, R.L. Terpstra, O. Unal, J. Electron. Mater. 30 (2001) 1050.
[8] M.G. Cho, S.K. Kang, D.Y. Shih, H.M. Lee, J. Electron. Mater. 36 (2007) 1501.
[9] Y.W. Wang, Y.W. Lin, C.T. Tu, C.R. Kao, J. Alloys Compd. 478 (2009) 121.
[10] S.C. Yang, C.C. Chang, M.H. Tsai, C.R. Kao, J. Alloys Compd. 499 (2010) 149.
[11] Y.W. Wang, C.C. Chang, C.R. Kao, J. Alloys Compd. 478 (2009) L1.
[12] Y.W. Wang, Y.W. Lin, C.R. Kao, J. Alloys Compd. 493 (2010) 233.
[13] Y.W. Wang, C.C. Chang, W.M. Chen, C.R. Kao, J. Electron. Mater. 39 (2010) 2636.
[14] Y.W. Wang, Y.W. Lin, C.R. Kao, Microelectron. Reliab. 49 (2009) 248.
[15] S.C. Yang, Y.W. Wang, C.C. Chang, C.R. Kao, J. Electron. Mater. 37 (2008) 1591.
[16] S.C. Yang, C.E. Ho, C.W. Chang, C.R. Kao, J. Mater. Res. 21 (2006) 2436.
[17] W. Liu, P. Bachorik, N.C. Lee, IEEE Electron. Compon. Technol. Conf. 58 (2008) 452.
[18] V. Vuorinen, H.Q. Dong, T. Laurila, J. Mater. Sci. 22 (2011) (online).
[19] P.A. Gruber, D. Shih, L. Belanger, G. Brouillette, D. Danovitch, V. Oberson, M. Turgeon, H. Kimura, IEEE Electron. Compon. Technol. Conf. 54 (2004) 650.
[20] M.G. Cho, H.Y. Kim, S.K. Seo, H.M. Lee, Appl. Phys. Lett. 95 (2009) 021905.
[21] J. Wang, C. Liu, C. Leinenbach, U.E. Klotz, P.J. Uggowitzer, J.F. Loffler, Calphad: Comput. Coupling Phase Diagrams Thermochem. 35 (2011) 82.
[22] X. Zhang, Y. Zhan, Q. Guo, G. Zhang, J. Hu, J. Alloys Compd. 480 (2009) 382.
[23] H. Kleinke, M. Waldeck, P. Gutlich, Chem. Mater. 12 (2000) 2219.
[24] B.B. Alchagirov, A.M. Chochaeva, High Temp. 38 (2000) 44.
[25] C. Coston, N.H. Nachtrieb, J. Phys. Chem. 68 (1964) 2219.